Supersymmetry spectroscopy in stop-chargino production at CERN LHC

M. Beccaria,[1,2] G. Macorini,[3,4] L. Panizzi,[3,4] F. M. Renard,[5] and C. Verzegnassi[3,4]
[1]*Dipartimento di Fisica, Università di Lecce, Via Arnesano, 73100 Lecce, Italy.*
[2]*INFN, Sezione di Lecce*
[3]*Dipartimento di Fisica Teorica, Università di Trieste, Strada Costiera 14, Miramare (Trieste)*
[4]*INFN, Sezione di Trieste*
[5]*Laboratoire de Physique Théorique et Astroparticules, UMR 5207, Université Montpellier II, F-34095 Montpellier Cedex 5*
(Received 6 October 2006; published 27 November 2006)

We consider the process of associated stop-chargino production in the MSSM at LHC and show that, at the simplest Born level, the production rate is dramatically sensitive to the choice of the benchmark points, oscillating from potentially visible maxima of the picobarn size to much smaller, hardly visible, values. Adopting a canonical choice of SM-type CKM matrices, we also show that in some visible cases the total rate exhibits a possibly relevant dependence on $\tan\beta$.

DOI: 10.1103/PhysRevD.74.093009 PACS numbers: 12.15.−y, 12.15.Lk, 13.75.Cs, 14.80.Ly

I. INTRODUCTION

Among the various processes that will be explored at LHC, the single top production, represented in Fig. 1, exhibits the interesting feature of providing the possibility of measuring the CKM V_{tb} matrix element, that appears already at Born level in the related cross ection, and for a recent study of this process in the MSSM we defer to the existing literature [1,2]. In a supersymmetric scenario, a similar property characterizes the three processes of single stop production, represented in Fig. 2 and called in this paper, in analogy with the single top case, *s*-channel, *t*-channel and associated stop-chargino production. As stressed in a very recent work [3], from these processes one could obtain a measurement of some of the CKM SUSY-SUSY matrix elements that appear already at Born level, i.e. a test of the usual SM-type assumptions. For this process, in particular, the analysis of [3] considers one special benchmark point (SPS5) and examines the potential effects of a deviation of the CKM matrix elements from their SM-like values, finding sizable effects in the considered parameter range.

Previous papers have already considered the mixed stop antisquark production [4] and the associated stop-chargino production case [5]. In Ref. [5] the process has been studied at NLO SUSY-QCD and LO electroweak level, finding a rather sizable one-loop QCD effect, that depends very strongly on the chosen value of $\tan\beta$, that appears at Born level.

The calculations of [5] have been performed for a rather special choice of parameters, in particular, using as input a negative value $\mu = -200$ GeV. From recent experimental analyses, the nowadays favored μ value appears to be positive if one assumes the most recent cosmological constraints on the dark matter relic density (see, for a very recent discussion [6]). Given the fact that the $\tan\beta$ dependence of the stop-chargino rate appears to be very strong, we feel that it might be interesting to reconsider the analysis of [5] starting from positive μ values. More specifically, the aim of this paper is that of generalizing the analysis of Refs. [3,5] to a wider class of SUSY benchmark points with positive μ. Our main goal is that of understanding the kind of $\tan\beta$ dependence that appears in the total rate. With

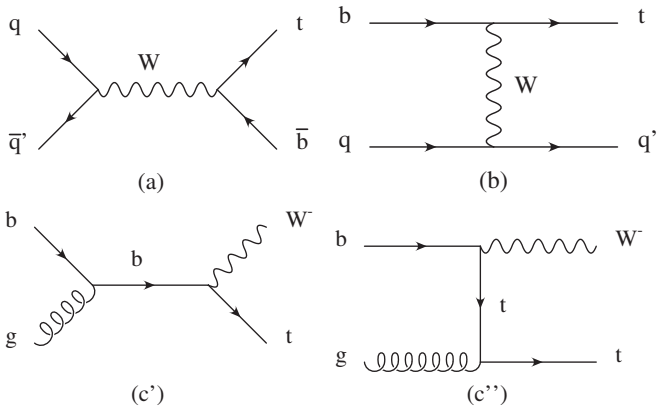

FIG. 1. Born diagrams for single top production: (a) *s*-channel, (b) *t*-channel, $(c') + (c'')$ associated production.

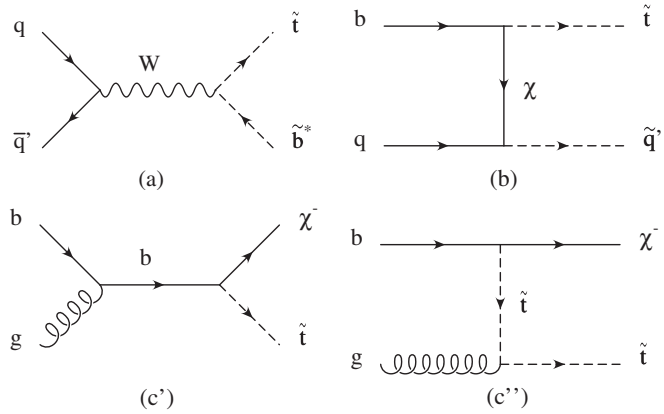

FIG. 2. Born diagrams for single stop quark production. They are in 1–1 correspondence with the diagrams of the previous Figure.

this aim, we shall only consider in this preliminary paper a description given at Born level, and we summarize quickly the results that we have obtained in Sec. II, essentially devoted to the kinematics of the process, and in Sec. III, where we show the main results of our study. A short final discussion will be given in Sec. IV. In Appendix A, we report the explicit form of the helicity amplitudes for the process $bg \to \tilde{t}_a \chi_i^-$ at Born level. In Appendix B, we give the high energy limit of the one-loop electroweak corrections.

II. KINEMATICAL DESCRIPTION OF THE PROCESS

The starting point is the expression of the invariant scattering amplitude for $bg \to \tilde{t}_a \chi_i^-$. In the notation of [1] we shall therefore write (factorizing out the color matrix elements), the s-channel and u-channel Born contributions:

$$A^{\mathrm{Born}(s)} = -\frac{g_s}{s - m_b^2}\bar{v}_c(\chi_i^-)[A_i^L(\tilde{t}_a)P_L + A_i^R(\tilde{t}_a)P_R](\not{q} + m_b)\not{\epsilon}u(b) \quad (1)$$

$$A^{\mathrm{Born}(u)} = -\frac{2g_s}{u - m_{\tilde{t}_a}^2}\bar{v}_c(\chi_i^-)[A_i^L(\tilde{t}_a)P_L + A_i^R(\tilde{t}_a)P_R] \times (e.p_{\tilde{t}_a})u(b) \quad (2)$$

where e^μ is the gluon polarization vector, $q = p_g + p_b$, $s = (p_b + p_g)^2$, $u = (p_b - p_{\chi_i^-})^2$ and $\alpha_s = \frac{g_s^2}{4\pi}$. The chargino states are χ_i^-, $i = 1, 2$ whereas $\tilde{t}_a$, $a = 1, 2$ are the physical stop states obtained from a mixing of the chiral fields $\tilde{t}_n$, $n = L, R$, such that

$$A_i^{L,R}(\tilde{t}_a) = R_{an}A_i^{L,R}(\tilde{t}_n) \quad (3)$$

with

$$R_{1L} = R_{2R} = \cos\theta_t \qquad R_{1R} = -R_{2L} = \sin\theta_t \quad (4)$$

The basic couplings

$$A_i^L(\tilde{t}_L) = -\frac{e}{s_W}Z_{1i}^+ \qquad A_i^L(\tilde{t}_R) = \frac{em_t}{\sqrt{2}M_W s_W \sin\beta}Z_{2i}^+$$
$$A_i^R(\tilde{t}_L) = \frac{em_b}{\sqrt{2}M_W s_W \cos\beta}Z_{2i}^{-*} \quad (5)$$

involve the chargino mixing matrices $Z_{ki}^\pm$ defined in [7] and controlling the gaugino-higgsino composition of charginos; note the direct sensitivity on $\tan\beta$ appearing in the higgsino components.

Starting from the previous equations and decomposing the Dirac spinors and the gluon polarization vector into helicity states λ_b, λ_χ, λ_g, one can easily derive the expression of the differential partonic cross section in terms of the eight possible helicity amplitudes computed in Appendix A (we retain the bottom mass, that cannot be neglected in a MSSM coupling scenario):

$$\frac{d\sigma^{\mathrm{Born}}}{d\cos\theta} = \frac{\beta'}{768\pi s\beta}\sum_{\lambda_b,\lambda_g,\lambda_\chi}|F^{\mathrm{Born}}_{\lambda_b,\lambda_g,\lambda_\chi}|^2$$

with $\beta = \frac{2p}{\sqrt{s}}$, $\beta' = \frac{2p'}{\sqrt{s}}$, p, p' being the initial and final c.m. momenta. The center of mass scattering angle θ is defined as the angle between the final stop squark and the initial bottom quark.

This partonic cross-section gets simple expressions in two limiting cases (a) at low energy (near above the threshold $\sqrt{s_{\mathrm{th}}} = m_\chi + m_{\tilde{t}}$), (b) at high energy ($\sqrt{s} \gg m_\chi, m_{\tilde{t}}$):

(a)

$$\frac{d\sigma^{\mathrm{Born}}}{d\cos\theta} = \frac{\alpha_s m_\chi \beta'}{96 s^{3/2}\beta}[|A_i^L(\tilde{t}_a)|^2 + |A_i^R(\tilde{t}_a)|^2], \quad (6)$$

(b)

$$\frac{d\sigma^{\mathrm{Born}}}{d\cos\theta} = \frac{\alpha_s \beta'^3}{96 s\beta}[|A_i^L(\tilde{t}_a)|^2 + |A_i^R(\tilde{t}_a)|^2]\sin^2\frac{\theta}{2}. \quad (7)$$

The low energy approximation is feeded by the helicity amplitudes F_{+++}, F_{---} and F_{++-}, F_{--+} and only the s-channel contribution (the u-channel contribution vanishes more rapidly at low energy because of an additional β' factor coming from the product $e \cdot p_{\tilde{t}_a}$).

The high energy approximation is only feeded by the u-channel amplitudes F_{-++}, F_{+--}. All the other ones are mass suppressed (like $m/\sqrt{s}$ or m^2/s) by kinematical factors or gauge cancellations between s and u-channel amplitudes. All these properties can easily be inferred from the detailed expressions listed in Appendix A. In Appendix B, we have also written the expressions of the one-loop electroweak corrections arising at logarithmic level from the so-called Sudakov terms [8], valid only in the very high energy limit.

It is remarkable that the information brought by this partonic cross section takes the form of

$$|A_i^L(\tilde{t}_a)|^2 + |A_i^R(\tilde{t}_a)|^2, \quad (8)$$

which, e.g. for the lighest stop quark $\tilde{t}_1$, reads

$$\cos^2\theta_t|A_i^L(\tilde{t}_L)|^2 + \sin^2\theta_t|A_i^L(\tilde{t}_R)|^2 + 2\sin\theta_t\cos\theta_t A_i^L(\tilde{t}_L)A_i^L(\tilde{t}_R) + \cos^2\theta_t|A_i^R(\tilde{t}_L)|^2, \quad (9)$$

which involves the 4 parameters θ_t, $\phi_{L,R}$ (that appear in the chargino mixing matrices [7]), and $\tan\beta$.

A disentangling of these various elements could be achieved if the polarization of the produced chargino could be measured (for instance from its decay products [9]). At low energy, $\lambda_\chi = +\frac{1}{2}$ is fed F_{+++} and F_{--+} which only depend on $A_i^R(\tilde{t}_a)$ at $\theta = 0$ and only on $A_i^L(\tilde{t}_a)$ at $\theta = \pi$.

Conversely, $\lambda_\chi = -\frac{1}{2}$ is fedby F_{---} and F_{++-} and only depends on $A_i^L(\tilde{t}_a)$ at $\theta = 0$ and only on $A_i^R(\tilde{t}_a)$ at $\theta = \pi$. At high energy, $\lambda_\chi = +\frac{1}{2}$ is only fed by F_{-++} and $A_i^L(\tilde{t}_a)$, whereas $\lambda_\chi = -\frac{1}{2}$ is produced by F_{+--} and $A_i^L(\tilde{t}_a)$. In both limiting cases this would allow a good check of the stop and chargino parameters. For the moment we shall only concentrate in this paper on the cross-section and its measurability at LHC.

III. PHYSICAL OBSERVABLES

The physically meaningful quantities are obtained by integrating over the angle with the available parton distribution functions. As a first observable, we considered the inclusive differential cross section, defined as:

$$\frac{d\sigma(PP \to \tilde{t}_a \chi_i^- + X)}{ds} = \frac{1}{S} \int_{\cos\theta_{\min}}^{\cos\theta_{\max}} d\cos\theta L_{bg}(\tau, \cos\theta) \times \frac{d\sigma_{bg\to\tilde{t}_a\chi_i^-}}{d\cos\theta}(s), \quad (10)$$

where $\tau = \frac{s}{S}$, and L_{bg} is the parton process luminosity.

$$L_{bg}(\tau, \cos\theta) = \int_{\bar{y}_{\min}}^{\bar{y}_{\max}} d\bar{y}[b(x)g(\tau/x) + g(x)b(\tau/x)] \quad (11)$$

where S is the total PP c.m. energy, and $i(x)$ the distributions of the parton i inside the proton with a momentum fraction, $x = \sqrt{\frac{s}{S}}e^{\bar{y}}$, related to the rapidity $\bar{y}$ of the $\tilde{t}_a\chi_i^-$ system [10]. The parton distribution functions are the Heavy quark CTEQ6 set [11]. The rapidity and angular integrations are performed after imposing a cut $p_T \geq 10$ GeV (see [12] for more details).

At least in the initial LHC period, a more meaningful quantity might be the integrated cross section. We considered here the integration from threshold to a variable final c.m. energy and allowed it to vary up to a final illustrative value of 2 TeV. Note that, moving to the one-loop level, the Born equality between the final c.m. energy and the physically meaningful final invariant mass is lost. The relationship between the two quantities can be obtained with a specific dedicated analysis analogous to the one performed in [12]. We expect from that reference that the difference should not be large. This feature will be examined in details in a forthcoming paper.

In our calculation, we considered a number of benchmark points. Our choice priviledged some special cases of couples of points whose main difference was the value of $\tan\beta$. For example the two points LS1 and LS2 defined by us in [1] exhibit an almost identical spectrum of physical masses, with $\tan\beta$ equal to 10 (LS1) and 50 (LS2). An analogous situation, although with slightly larger mass differences, characterizes the two points SU1 and SU6 [13]. To have a check of our calculation, we also considered the Snowmass benchmark point SPS5 [14] used in Ref. [3] which has $\tan\beta = 5$. For our purposes, we varied $\tan\beta$ within this point, moving to the final (allowed) value of $\tan\beta = 40$. The mSUGRA parameters associated with these points are reported in Table I.

TABLE I. mSUGRA parameters for the benchmark points LS1, LS2, SU1, SU6, and SPS5. All masses are expressed in GeV.

	m_0	$m_{1/2}$	A_0	$\tan\beta$	sign(μ)
LS1	300	150	−500	10	+
LS2	300	150	−500	50	+
SU1	70	350	0	10	+
SU6	320	375	0	50	+
SPS5	150	300	−1000	5	+
SPS5a	150	300	−1000	15	+
SPS5b	150	300	−1000	40	+

To have a feeling of the different relevant stops, charginos masses in the various benchmark points, we have shown them in Fig. 3. As one sees, the mass spectra are almost identical in LS1 and LS2, and roughly identical in SU1 and SU6. In the next Figures, we show the results of our calculation.

Figures 4–6 show the inclusive differential cross sections for the three pairs of points. For simplicity, we only show the results that correspond to the lightest final pair $(\tilde{t}, \chi)$. We can anticipate the fact that in the three remaining possibilities the distributions are greatly reduced, with the possible exception of the combination of the lightest stop squark and heavier chargino in LS1, LS2 cases. As one sees, in all considered cases the common feature is that of a sensible dependence on $\tan\beta$. This is due to the combination of two quite distinct effects. First, the mass spectrum and, as a consequence, the threshold for the production of a $\tilde{t}\chi$ state clearly depend on $\tan\beta$. Of course, a high threshold implies a strong reduction of the cross-section. This kind of effect can be observed if we compare the benchmark points SU1 and SU6 or also SPS5/SPS5a and SPS5b. Secondly, an additional $\tan\beta$-dependence enters through

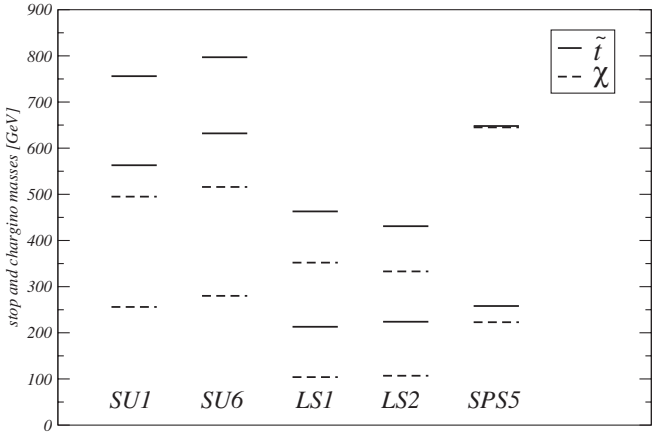

FIG. 3. Chargino and stop masses in the considered benchmark points LS1, LS2, SU1, SU6 and SPS5.

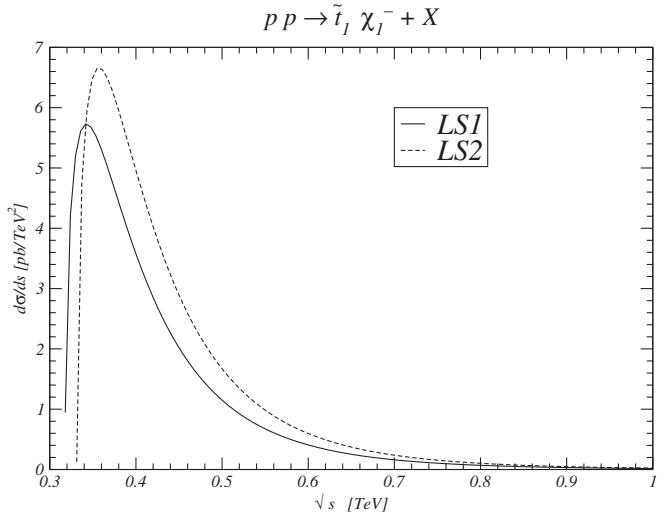

FIG. 4. Differential distribution $d\sigma/ds$ for producing the lightest $\tilde{t}\chi$ final state at the benchmark points LS1, LS2.

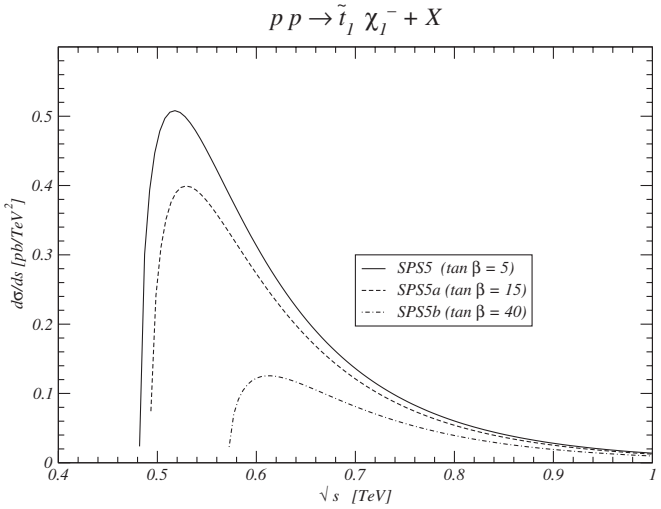

FIG. 6. Differential distribution $d\sigma/ds$ for producing the lightest $\tilde{t}\chi$ final state at the benchmark points SPS5, SPS5a, SPS5b.

the appearance of that parameter in the couplings $A_i^{L,R}$. This second kind of effect can be observed clearly in those cases where the variation of $\tan\beta$ does not lead to large changes in the threshold. Examples can be found in the comparison between the benchmark points LS1 and LS2 or SPS5 and SPS5a.

A detailed analysis of these two cases is worth ones while in order to understand why the cross section increases with $\tan\beta$ in the first case (LS1/LS2) whereas it decreases in the second one (SPS5/SPS5a). Starting with LS1/LS2, we show in Fig. 7 the distribution $d\sigma/ds$ for the various helicity components as $\sqrt{s}$ increases. In the peak region, there are two dominant contributions with the specific (sign of) helicity combinations $--+$ and $---$ whereas at higher energy, only the $-++$ term survives. When $\tan\beta$ is increased, the dominant channels tend to decrease slightly. They receive a mixed contribution composed of a dominant gaugino coupling and a smaller higgsino one. The relative signs of the combinations are responsible for the decrease of this term when $\tan\beta$ is increased and the higgsino contribution grows. On the other hand, there are two channels with helicities $++-$ and $+++$ which are purely of higgsino origin. These are quite small in LS1 but sizable in LS2. They are responsible for the increase in the total $d\sigma/ds$. We do not show a similar figure for the case SPS5/SPS5a, but the mechanism

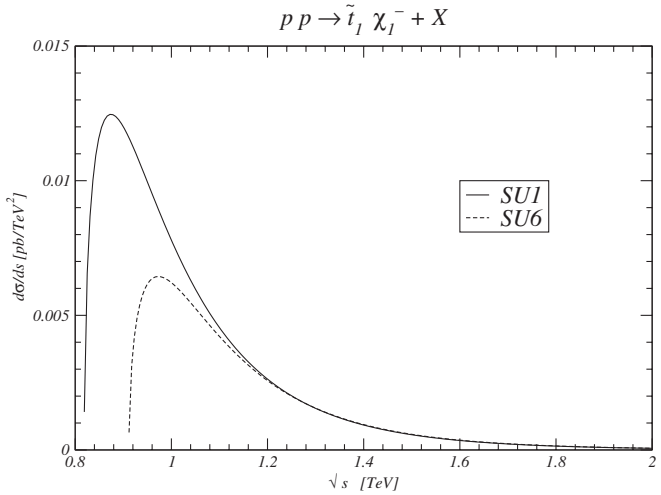

FIG. 5. Differential distribution $d\sigma/ds$ for producing the lightest $\tilde{t}\chi$ final state at the benchmark points SU1, SU6

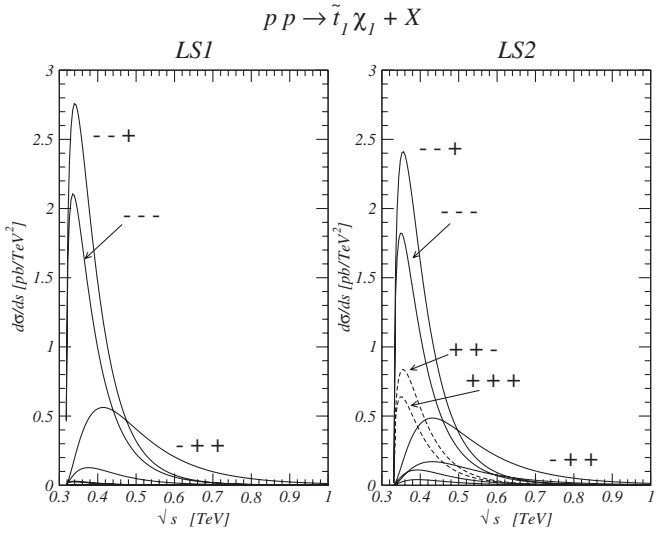

FIG. 7. Differential distribution $d\sigma/ds$ for producing the lightest $\tilde{t}\chi$ final state at the benchmark points LS1, LS2. We show all the separate helicity channels and label the most relevant ones. The labels show the sign of the helicities of the various involved particles in the order b quark, gluon, chargino. An angular cut $|\cos\theta| < 0.9$ has been applied to better separate the various lines. The dashed lines in the LS2 panel are those helicity components which are enhanced by the large $\tan\beta$ value.

is quite similar. The only difference is that now the $+\,+\,-$ and $+\,+\,+$ amplitudes are much smaller due to a combination of various effects (different $\tan\beta$ and mixing matrix elements). When $\tan\beta$ is increased from 5 to 15, the rise of these amplitudes is unable to invert the (negative) trend due to the leading amplitudes.

To make a more realistic analysis, we show in the next Figs. 8–10 the values of the integrated cross sections. From their inspection, two main conclusions can be, in our opinion, derived. The first one concerns the magnitude of the various rates. We assume, for simplicity, that a value of one picobarn for the rate corresponds, roughly and for the expected luminosity, to ten thousands events per year. In this sense, we consider it as a reasonable experimentally meaningful limit, leaving aside in this qualitative discussion identification details. For rate values drastically below the picobarn size, the process might still be ''visible'' but hardly exploitable in our opinion for a meaningful parameter analysis.

Keeping in mind our qualitative classification, we see that the rates of the three point couples oscillate from a maximum of the picobarn size (LS1, LS2) to a minimum of $\simeq 10^{-2}$ picobarn (SU1, SU6), passing through an intermediate stage of $\simeq 10^{-1}$ picobarn (SPS5) (in fact, all our results should be multiplied by a factor of 2, to keep into account the conjugate state $\chi^{+}\tilde{t}^{*}$, produced by an initial $\bar{b}g$ pair, whose rate is essentially identical with that of $\chi^{-}\tilde{t}$). As one sees, the rate variations from one pair to another one are of 1 order of magnitude. We should also say as a check of our calculations, that our results for SPS5 reproduce essentially the corresponding SM type one (defined ''plain'') of Ref. [3].

The second main comment is that, in all three cases, the variations of the rate with $\tan\beta$ are not small. More precisely, they are of the relative 30% size for LS1, LS2 and of the relative 60% size for SU1, SU6. In the case of SPS5, the variation with $\tan\beta$ is the most drastic. Moving from $\tan\beta = 5$ to $\tan\beta = 40$ would change the rate by a factor of 3 that would hardly escape an experimental detection.

We remark that this rather strong $\tan\beta$ dependence is observable despite the gaugino character of the lightest chargino, a general feature of mSUGRA benchmark points with a light stop. Moving onward to more general symmetry breaking schemes, any point characterized by a light stop and an higgsinolike lightest chargino would enhance the discussed sensitivity. This would be precisely the case of [5], since their choice of the parameters selects, as one can easily check, a lightest chargino with a sizable higgsino component.

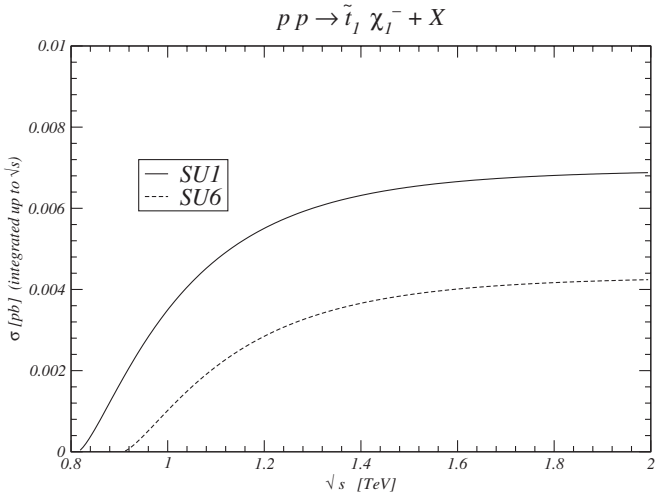

FIG. 9. Integrated cross section from threshold up to $\sqrt{s}$ for the production of the lightest $\tilde{t}\chi$ final state. Benchmark points: SU1, SU6.

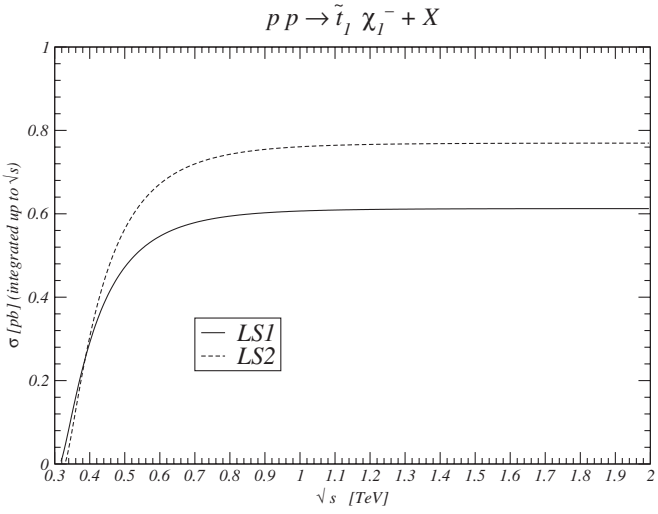

FIG. 8. Integrated cross section from threshold up to $\sqrt{s}$ for the production of the lightest $\tilde{t}\chi$ final state. Benchmark points: LS1, LS2.

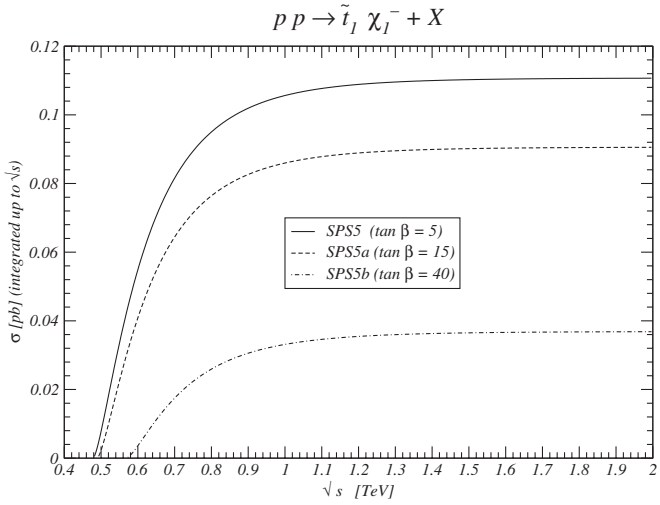

FIG. 10. Integrated cross section from threshold up to $\sqrt{s}$ for the production of the lightest $\tilde{t}\chi$ final state. Benchmark points: SPS5, SPS5a, SPS5b.

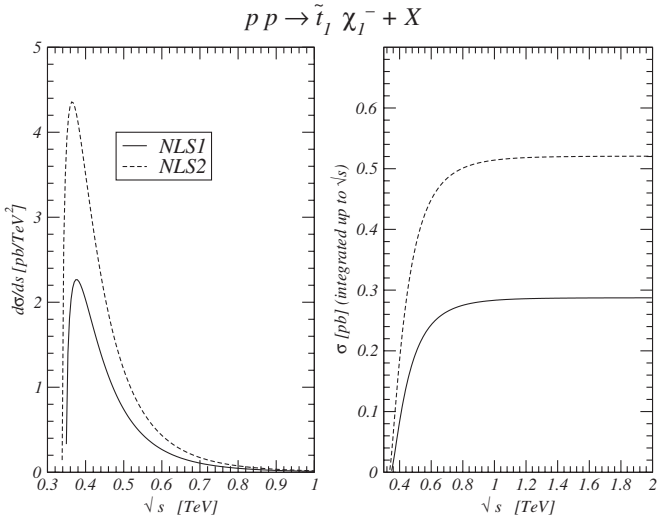

FIG. 11. Differential distribution $d\sigma/ds$ and integrated cross section from threshold up to $\sqrt{s}$ for the production of the lightest $\tilde{t}\chi$ final state. The benchmark points are NLS1, NLS2, both with $\mu < 0$.

A final possibly interesting question that we try to face is the dependence of the rate on the assumed sign of the μ parameter (this could become relevant only if the existing cosmological constraint were removed). To give a quantitative example of the potential effects of a change in the sign of μ, we have redone some of our calculations changing the sign of the μ value. Figs. 11 and 12 show the results in the two "more observable" cases LS1/LS2 and SPS5/SPS5a. The associated benchmark points with *negative* $\mu < 0$ (and the same $|\mu|$) are defined NLS1, NLS2, NSPS5, and NSPS5a. As one sees, the $\tan\beta$ dependence is strongly enhanced in the two cases, increasing by almost

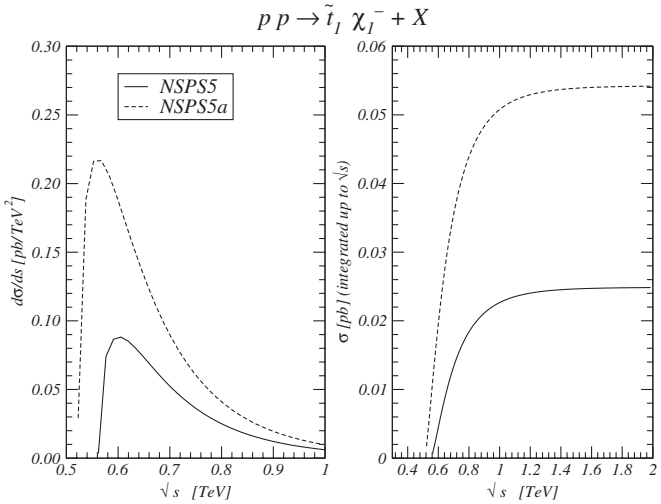

FIG. 12. Differential distribution $d\sigma/ds$ and integrated cross section from threshold up to $\sqrt{s}$ for the production of the lightest $\tilde{t}\chi$ final state. The benchmark points are NSPS5, NSPS5a, both with $\mu < 0$.

a factor 2 with respect to the positive μ analysis, while the size of the total rate is only slightly decreased, at least for large $\tan\beta$. Note that even with a negative μ the lightest chargino is still of essentially gaugino type due to the natural $|\mu| \gg M_2$ hierarchy, contrary to the case of [5].

IV. CONCLUSIONS

In conclusion, we have seen that the process of stop-chargino production appears, in a light stop-chargino scenario, to be a possible promising candidate for a "spectroscopic" test of different SUSY scenarios and also, possibly, for a measurement of $\tan\beta$. In this respect, it would represent an alternative possibility to those offered by more conventional and direct measurements in the Higgs sector. For instance, at LHC, $\tan\beta$ can be determined from a study of the production process $gg \to b\bar{b}H/A/h$ which is the dominant Higgs boson production process at large $\tan\beta$ [15]. From an analysis of the subsequent Higgs decays (mainly $H/A/h \to \tau\tau \to jj + X$ or $H/A/h \to \tau\tau \to \ell j + X$) performed at 30 fb^{-1} it is possible to determine $\tan\beta$ with a statistical error 4–25% and a systematic error $\leq 12\%$ depending on the signal significance [16].

To complete this preliminary study, two main analyses are still missing, The first one is a realistic experimental discussion of the expected errors. To our knowledge, preliminary experimental analyses of light stop-antistop pairs production have been very recently provided [17]. In our opinion, their extension to the stop-chargino case could be interesting. The second one is a complete NLO theoretical calculation, which would be justified by the presence of a large $\tan\beta$ dependence at Born level. For what concerns the NLO QCD analysis for a more general set of input parameters, in particular, with $\mu > 0$, we think that the analysis of [5] should be redone, but an essential point, in our opinion, would be the additional and combined calculation of the one-loop electroweak effects, since *a priori* the $\tan\beta$ dependence might be sensibly modified at this level, particularly in a light stop-chargino scenario where sizable electroweak logarithmic effects of Sudakov kind shown in Appendix B might arise from one-loop diagrams. Our group is already proceeding in the complete one-loop electroweak calculation.

APPENDIX A: BORN LEVEL HELICITY AMPLITUDES

The Born level helicity amplitude is

$$F_{\lambda_b\lambda_g\lambda_\chi} = \sum_{\substack{\eta=L,R \\ k=1,2}} N_k^\eta \mathcal{H}^\eta_{k,\lambda_b\lambda_g\lambda_\chi}, \tag{A1}$$

where

$$N_1^\eta = -g_s \frac{A_i^\eta(\tilde{t}_a)}{s - m_b^2}, \qquad N_2^\eta = 2g_s \frac{A_i^\eta(\tilde{t}_a)}{u - m_{\tilde{t}_a}^2}, \tag{A2}$$

and

$$\mathcal{H}^{\eta}_{1,+++} = -\frac{pR}{\sqrt{2}}(1+r_b)(1+\eta)(1-r_\chi)\cos\frac{\theta}{2} \quad \text{(A3)}$$

$$\mathcal{H}^{\eta}_{1,++-} = -\frac{pR}{\sqrt{2}}(1+r_b)(1+\eta)(1+r_\chi)\sin\frac{\theta}{2} \quad \text{(A4)}$$

$$\mathcal{H}^{\eta}_{1,--+} = \frac{pR}{\sqrt{2}}(1+r_b)(1-\eta)(1+r_\chi)\sin\frac{\theta}{2} \quad \text{(A5)}$$

$$\mathcal{H}^{\eta}_{1,---} = -\frac{pR}{\sqrt{2}}(1+r_b)(1-\eta)(1-r_\chi)\cos\frac{\theta}{2} \quad \text{(A6)}$$

$$\mathcal{H}^{\eta}_{2,+++} = -\frac{p'R\sin\theta}{2\sqrt{2}}(1+\eta r_b - r_\chi(\eta+r_b))\sin\frac{\theta}{2} \quad \text{(A7)}$$

$$\mathcal{H}^{\eta}_{2,+-+} = \frac{p'R\sin\theta}{2\sqrt{2}}(1+\eta r_b - r_\chi(\eta+r_b))\sin\frac{\theta}{2} \quad \text{(A8)}$$

$$\mathcal{H}^{\eta}_{2,++-} = \frac{p'R\sin\theta}{2\sqrt{2}}(1+\eta r_b + r_\chi(\eta+r_b))\cos\frac{\theta}{2} \quad \text{(A9)}$$

$$\mathcal{H}^{\eta}_{2,+--} = -\frac{p'R\sin\theta}{2\sqrt{2}}(1+\eta r_b + r_\chi(\eta+r_b))\cos\frac{\theta}{2} \quad \text{(A10)}$$

$$\mathcal{H}^{\eta}_{2,-++} = \frac{p'R\sin\theta}{2\sqrt{2}}(1-\eta r_b - r_\chi(\eta-r_b))\cos\frac{\theta}{2} \quad \text{(A11)}$$

$$\mathcal{H}^{\eta}_{2,--+} = -\frac{p'R\sin\theta}{2\sqrt{2}}(1-\eta r_b - r_\chi(\eta-r_b))\cos\frac{\theta}{2} \quad \text{(A12)}$$

$$\mathcal{H}^{\eta}_{2,-+-} = \frac{p'R\sin\theta}{2\sqrt{2}}(1-\eta r_b + r_\chi(\eta-r_b))\sin\frac{\theta}{2} \quad \text{(A13)}$$

$$\mathcal{H}^{\eta}_{2,---} = -\frac{p'R\sin\theta}{2\sqrt{2}}(1-\eta r_b + r_\chi(\eta-r_b))\sin\frac{\theta}{2} \quad \text{(A14)}$$

The kinematical parameters R, r_b, and r_χ appearing in the above expressions are defined as

$$R = \sqrt{(E_b+m_b)(E_\chi+m_\chi)}, \quad \text{(A15)}$$

$$r_b = \frac{p}{E_b+m_b}, \quad \text{(A16)}$$

$$r_\chi = \frac{p'}{E_\chi+m_\chi}, \quad \text{(A17)}$$

where E_b and E_χ are the b quark and chargino c.m. energies.

APPENDIX B: ONE-LOOP ELECTROWEAK CORRECTIONS AT LOGARITHMIC LEVEL

From the general rules given in [8] we can already give the expressions of these corrections due to the so-called Sudakov terms. These expressions should only be valid in the domain $\sqrt{s} \gg m_{\tilde{t}}, m_\chi$. At low energy, a dedicated complete one-loop calculation is necessary and is under way.

$$F^{\text{Sudakov}}_{-++}(\tilde{t}_L) = F^{\text{Born}}_{-++}(\tilde{t}_L)\frac{\alpha}{4\pi}\left\{\frac{1+26c_W^2}{36s_W^2c_W^2}\left(2\log\frac{s}{M_W^2} - \log^2\frac{s}{M_W^2}\right) + -\frac{1}{s_W^2}\log\frac{s}{M_W^2}\left[2\log\frac{-u}{s} + \frac{1-10c_W^2}{18s_W^2c_W^2}\log\frac{-t}{s}\right] + -\log\frac{s}{M_W^2} \times\left[\frac{m_t^2(1+\cot^2\beta)}{2s_W^2M_W^2} + \frac{m_b^2(1+\tan^2\beta)}{2s_W^2M_W^2}\right]\right\} \quad \text{(B1)}$$

$$F^{\text{Sudakov}}_{-++}(\tilde{t}_R) = F^{\text{Born}}_{-++}(\tilde{t}_R)\frac{\alpha}{4\pi}\left\{-\frac{13+14c_W^2}{36s_W^2c_W^2}\log^2\frac{s}{M_W^2} + -\frac{1}{6c_W^2}\log\frac{s}{M_W^2}\left[\frac{4}{3}\log\frac{-t}{s} - \frac{1-10c_W^2}{s_W^2}\log\frac{-u}{s}\right]\right\} \quad \text{(B2)}$$

$$F^{\text{Sudakov}}_{+--}(\tilde{t}_L) = F^{\text{Born}}_{+--}(\tilde{t}_L)\frac{\alpha}{4\pi}\left\{-\frac{7+20c_W^2}{36s_W^2c_W^2}\log^2\frac{s}{M_W^2} + -\frac{1}{3c_W^2}\log\frac{s}{M_W^2}\left[\log\frac{-u}{s} - \frac{1}{3}\log\frac{-t}{s}\right]\right\} \quad \text{(B3)}$$

[1] M. Beccaria, G. Macorini, F. M. Renard, and C. Verzegnassi, Phys. Rev. D **73**, 093001 (2006).

[2] M. Beccaria, G. Macorini, F. M. Renard, and C. Verzegnassi, Phys. Rev. D **74**, 013008 (2006).

[3] B. Fuks, Talk presented at the 3rd Workshop On the Interplay of Flavor and Collider Physics, CERN, Geneva, 2006.
[4] G. Bozzi, B. Fuks, and M. Klasen, Phys. Rev. D **72**, 035016 (2005).
[5] L. G. Jin, C. S. Li, and J. J. Liu, Eur. Phys. J. C **30**, 77 (2003); Phys. Lett. B **561**, 135 (2003).
[6] B. C. Allanach, C. G. Lester, and A. M. Weber, hep-ph/0609295.
[7] J. Rosiek, Phys. Rev. D **41**, 3464 (1990).
[8] M. Beccaria, M. Melles, F. M. Renard, S. Trimarchi, and C. Verzegnassi, Int. J. Mod. Phys. A **18**, 5069 (2003).
[9] S. Y. Choi, A. Djouadi, H. K. Dreiner, J. Kalinowski, and P. M. Zerwas, Eur. Phys. J. C **7**, 123 (1999).
[10] see e.g. R. K. Ellis, W. J. Stirling, and B. R. Webber, *QCD and Colliders Physics*, edited by T. Ericson and P. V. Landshoff (Cambridge University Press, Cambridge, England, 1996).
[11] S. Kretzer, H. L. Lai, F. I. Olness, and W. K. Tung, Phys. Rev. D **69**, 114005 (2004); Additional information about CTEQ6 parton distribution functions can be found in http://hep.pa.msu.edu/people/wkt/cteq6/cteq6pdf.html.
[12] M. Beccaria, S. Bentvelsen, M. Cobal, F. M. Renard, and C. Verzegnassi, Phys. Rev. D **71**, 073003 (2005).
[13] ATLAS Data Challenge 2 DC2 points: http://paige.home.cern.ch/paige/fullsusy/romeindex.html.
[14] B. C. Allanach *et al.*, Eur. Phys. J. C 25, 113 (2002).eConf C010630 (2001), p. P125.
[15] S. Dittmaier, M. Kramer, and M. Spira, Phys. Rev. D **70**, 074010 (2004).
[16] M. Hashemi, hep-ph/0504243.
[17] I. Borjanovic (ATLAS Collaboration), Proc. Sci. HEP2005 (2006) 350; I. Borjanovic, J. Krstic, and D. Popovic, Prepared for Conference on Physics at LHC, Vienna, Austria, 2004; Czech. J. Phys. **55**, B793 (2005).